NANO LETTERS

pubs.acs.org/NanoLett Letter

Imaging the Magnetic Anisotropy in Ultrathin Fe_4GeTe_2 with a Nitrogen-Vacancy Magnetometer

Chen Wang, Siyuan Wan, Ya Wang, Fazhan Shi,* Ming Gong,* and Hualing Zeng*

Cite This: *Nano Lett.* 2024, 24, 5754−5760 Read Online

ACCESS | Metrics & More | Article Recommendations | Supporting Information

ABSTRACT: Two-dimensional (2D) Fe_nGeTe_2, with n = 3, 4, and 5, has been realized in experiments, showing strong magnetic anisotropy with enhanced critical temperature (T_c). The understanding of its magnetic anisotropy is crucial for the exploration of more stable 2D magnets and its spintronic applications. Here, we report a quantitative reconstruction of the magnetization magnitude and its direction in ultrathin Fe_4GeTe_2 using nitrogen vacancy centers. Through imaging stray magnetic fields, we identified the spin-flop transition at approximately 80 K, resulting in a change of the easy axis from the out-of-plane direction to the in-plane direction. Moreover, by analyzing the thermally activated escape behavior of the magnetization near T_c in terms of the Ginzburg−Landau model, we observed the in-plane magnetic anisotropy effect and the formation capability of magnetic domains at ∼0.4 $\mu m^2\ \mu T^{-1}$. Our findings contribute to the quantitative understanding of the magnetic anisotropy effect in a vast range of 2D van der Waals magnets.

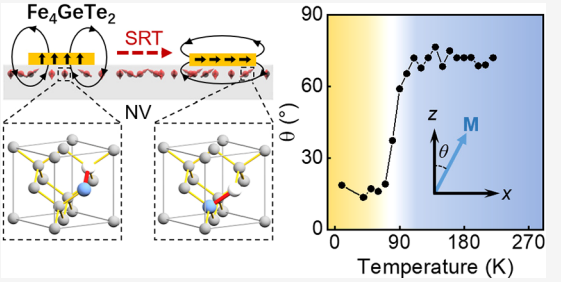

KEYWORDS: *NV centers, Fe_4GeTe_2, magnetic anisotropy, thermal-activated escape*

The discovery of two-dimensional (2D) van der Waals (vdW) magnets has opened up new possibilities for studying low-dimensional magnetic phase transitions and designing 2D spintronic devices.[1−7] However, the applications of most vdW magnets are limited by the relatively low critical temperatures (T_c). In recent years, 2D Fe_nGeTe_2 (n = 3, 4, 5) has attracted significant attention.[4,8−17] With increasing n, the spin-exchange interaction and anisotropy increase. Accordingly, the fluctuation effect is suppressed, leading to enhanced T_c, with T_c values of ∼220, 270, and 300 K for bulk materials with n = 3, 4, and 5, respectively. Furthermore, the anisotropy also leads to a spin reorientation transition (SRT) from out-of-plane magnetization to in-plane magnetization in Fe_4GeTe_2,[9,18] which may be useful for stabilizing magnetism in device applications. However, obtaining a quantitative description of their magnetic structures becomes increasingly complex and more challenging. To date, while the phase transition has been revealed,[19,20] the subtle magnetic anisotropy and the associated magnetization directions have not yet been fully identified.[21,22]

The nitrogen vacancy (NV) center in diamond, which can directly sense the magnetic field,[23−28] may provide an ideal experimental platform for investigating the SRT and the associated magnetic anisotropy. For example, a magnetometer based on NV ensembles enables the direct measurements of both the intensity and direction of external magnetic fields utilizing their four orientations within the diamond lattice. This tool possesses a number of advantages, such as a wide temperature range of operation[29,30] and high sensitivity.[31,32] With these benefits, the stray magnetic field from a wide range of 2D magnets including ultrathin CrI_3, $CrBr_3$, VI_3, and small-angle twisted bilayer CrI_3 has been imaged by NV centers very recently.[33−36] Moreover, in addition to reconstructing the magnetization strength, NV centers are sensitive to the stray field directions, allowing a quantitative study on the anisotropy of magnetization and the weak magnetic behavior near T_c for 2D magnets.

In this work, the stray magnetic field from a bilayer Fe_4GeTe_2 is imaged using an ensemble NV magnetometer. With the aid of an untrained physically informed neural network,[37,38] the strength and direction of magnetization are reconstructed. The major results are summarized as follows. First, we observe the easy-axis transition from the out-of-plane direction to the in-plane direction at approximately 80 K, which is slightly lower than the SRT temperature reported in refs 9 and 18. By quantitative measurements, we reveal the temperature dependent change in the zenith angle of the in-plane and out-of-plane magnetization. Second, when the temperature is slightly lower than T_c,[39−41] we observe the thermal-fluctuation-induced random switching of the in-plane magnetizations. This behavior is well understood as a thermally activated escape process within the Ginzburg−Landau (GL) theory by taking into account the in-plane anisotropy effect.

Received: February 14, 2024
Revised: April 26, 2024
Accepted: May 1, 2024
Published: May 6, 2024

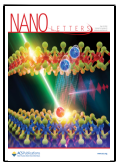

https://doi.org/10.1021/acs.nanolett.4c00795
Nano Lett. 2024, 24, 5754−5760

Under the tuning of a weak in-plane magnetic field, we quantitatively determine the in-plane easy-axis direction and the formation capability of magnetic domains ~0.4 $\mu m^2\ \mu T^{-1}$ near T_c. The method presented in this work provides an appealing experimental tool for qualitatively characterizing the magnetization and the subtle magnetic dynamics near the phase transition in 2D magnets.[42]

Our general idea is illustrated in Figure 1. In Figure 1a, we use a diamond with a near-surface layer of magnetically sensitive NV centers (a few nanometers thick and ~10 nm from the upper surface) as the magnetometer, which allows the measurement of the stray magnetic field $\mathbf{B}_s$ generated by the sample through scanning confocal imaging. Our mechanically exfoliated Fe_4GeTe_2 flake (see Section III in the Supporting Information) is transferred to the diamond surface and encapsulated with hexagonal boron nitride (hBN) on both sides. The top hBN layer prevents degradation, while the bottom hBN layer serves as a substrate, eliminating the artifact effect[43] (see Method in Section I of the Supporting Information). The Zeeman splitting of the NV centers is produced by the magnetic field component parallel to the NV axis and thus is independent of its perpendicular direction. Using the four different types of NV centers in diamond, the magnetic field strength and direction can be fully determined with this magnetometer.[23,44,45] Two typical Zeeman splittings for NV_1 and NV_2 from the optically detected magnetic resonance (ODMR) spectra are presented in Figure 1b. In principle, using the ODMR spectrum of each pixel and the direction of the NV axes, the intensity and direction of the magnetic field $\mathbf{B}_s$ can be measured, which can be used to reconstruct the surface magnetization in the sample.

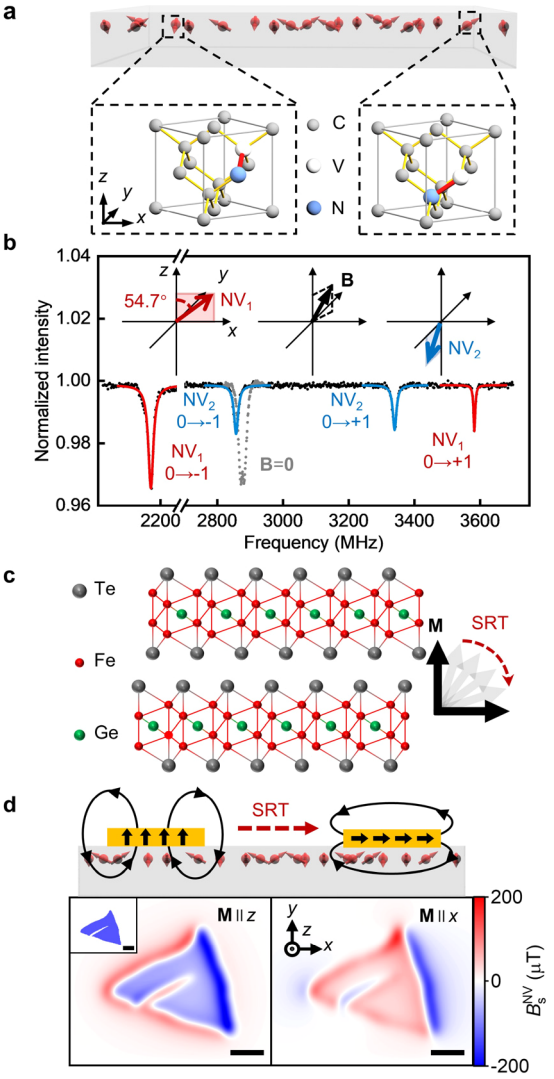

Figure 1. Magnetic resonance imaging with a NV center magnetometer. (a) Schematic of a diamond containing a near-surface NV layer. The two boxes show two typical NV centers with different axis directions. (b) ODMR spectrum for two typical NV centers NV_1 and NV_2 with (black dots) or without (gray dots) a magnetic field. The solid lines are the corresponding fitting with Lorentz curves. The insets show the axis directions of these centers. (c) Side view of the atomic lattice of Fe_4GeTe_2. The arrows indicate the possible magnetization directions. (d) SRT from the out-of-plane direction to the in-plane direction. The lower two figures are their corresponding calculated stray magnetic field B_s^{NV}, which can be directly determined by the NV centers. Parameters used are as follows: distance between NV and sample, 270 nm; surface magnetization, M = 60 μ_B nm^{-2}. Scale bars are 3 μm.

The crystal structure of Fe_4GeTe_2 is shown in Figure 1c, with a space group of $R\bar{3}m$. For each single layer, the thickness is ~1 nm, and a C_3 symmetry is expected. The 3-fold symmetry indicates that it may exhibit anisotropy within the in-plane direction.[9] Furthermore, the easy axis of Fe_4GeTe_2 changes from the out-of-plane to the in-plane direction during the SRT, which is significantly distinct from Fe_3GeTe_2 with the fixed magnetic easy axis in the out-of-plane direction. Figure 1d illustrates the schematic magnetic flux lines from in-plane or out-of-plane magnetizations. The different stray magnetic fields result in distinguished ODMR spectra. Therefore, by combining the distribution of the measured stray field B_s^{NV} (the projection of $\mathbf{B}_s$ along NV_1, with $NV_1 \approx 54.7°$ relative to the z axis; see the inset of Figure 1b) and the distance between the sample and the NV layer, the surface magnetization and direction and be reconstructed. For example, the magnetizations for a triangular domain under these two conditions are simulated in Figure 1d.

Figure 2a shows an optical image of a Fe_4GeTe_2 flake, which has a thickness of ~2 nm, as confirmed by atomic force microscopy measurement in Figure 2b. This sample is encapsulated in top hBN in a glovebox and then quickly transferred to a cryostat. The flake is cooled to 10 K under an external bias magnetic field of B_{bias}^{NV} = 25 mT along the NV_1 axis,[46,47] and then it is heated from 10 to 270 K by keeping B_{bias}^{NV} constant to explore the evolution of the stray magnetic field. More supporting data are presented in Section V in the Supporting Information. From Figure 2c, we see that the magnetic field distribution matches well with the sample geometry, without obvious magnetic domain wall structures, indicating that the sample is almost uniformly magnetized. We find that with increasing temperature, the stray field changes significantly, as indicated not only by the field intensity but also by the distribution of the stray field. By comparing the results in Figures 1d and 2c from 60 to 100 K, we find a gradual change of the stray field distribution, implying a SRT transition at ~80 K. A similar transition at ~100 K in Fe_4GeTe_2 has been reported elsewhere.[9,18]

To confirm the SRT transition, we reconstructed the surface magnetization using an untrained physically informed neural network processing via the method in ref 37 based on B_s^{NV} from NV_1 instead of $\mathbf{B}_s$ (for additional details, see Section VI in the Supporting Information). The results are presented in

https://doi.org/10.1021/acs.nanolett.4c00795
Nano Lett. 2024, 24, 5754−5760

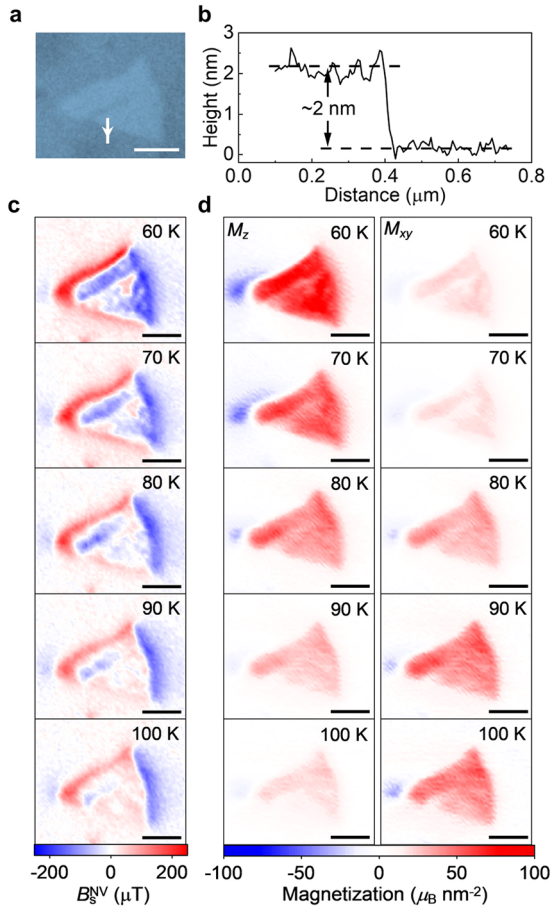

Figure 2. Stray magnetic field and magnetization at different temperatures. (a) Optical image of the Fe_4GeTe_2 flake on diamond before encapsulation by the top hBN. (b) Atomic force microscope image of the Fe_4GeTe_2 flake along the white arrow in (a). (c) Stray magnetic field and (d) the reconstructed out-of-plane and in-plane magnetizations using an untrained physically informed neural network at different temperatures. All scale bars are 5 μm.

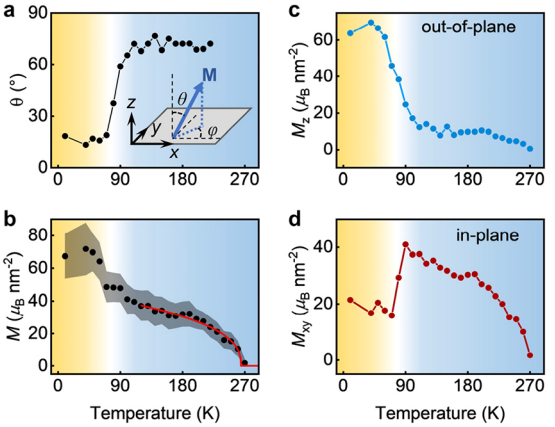

Figure 3. SRT and surface magnetization in Fe_4GeTe_2. (a) Zenith angle θ of the magnetization of the Fe_4GeTe_2 flake at different temperatures. The inset shows the zenith angle θ and azimuth angle φ. (b) Magnetization intensity of Fe_4GeTe_2 flakes at different temperatures. The black dots are the experimental data. The red line is fitted using $M \propto (1 - T/T_c)^{\beta}$, with the result of $T_c \approx 264.4 \pm 3.5$ K. The gray area is the error bar. (c) Out-of-plane and (d) in-plane magnetization intensities of Fe_4GeTe_2 flakes at different temperatures.

Figure 2d and are in accordance with the sample geometry. These results clearly demonstrate that in the range of 60−100 K, the in-plane magnetization intensity M_{xy} increases while the out-of-plane magnetization intensity M_z decreases with the increase in temperature due to the SRT.

With the reconstructed surface magnetization (more data in Section V in the Supporting Information), we can determine the direction and distribution of magnetization in the flake from 10 to 270 K. In Figure 3a, the zenith angle θ between the direction of magnetization and the z-axis is presented, showing that θ is ∼16° in the range of 10−60 K and ∼72° when $T >$ 100 K. The transition from out-of-plane to in-plane magnetization is manifested in the range of 60−100 K, which is consistent with the results in Figure 2. In addition, the azimuth angle φ, the angle between the in-plane magnetization and the x axis, is approximately 0° at all temperatures and is not shown. This is consistent with the projection of the external bias magnetic field in the xy plane, aligned with the x-axis. These results demonstrate that the SRT is not strictly oriented along the z axis or the xy plane, probably because of the effect of the external field $\mathbf{B}_{bias}$. We present the total magnetization M and its z and xy components M_z and M_{xy} in Figure 3b−d. We find that while the zenith angle may change in a relatively sharp way, the magnetizations may change in a relatively smooth way, indicating that the easy axis might rotate via a continuous spin-flopping transition rather than a discontinuous spin-flipping transition.[48] These two channels for the spin transitions are typical features in anisotropic magnetic materials, in which the spin-flop is a much smoother process in changing the spin direction. Furthermore, using the data in Figure 3a,b, and in the Stoner−Wohlfarth model, we present the effective magnetic anisotropy in Section IX in the Supporting Information. At 10 K, the effective magnetic anisotropy energy is estimated to be ∼0.01 J cm^{-3}, which is an order of magnitude smaller than that of bulk materials. This result is in consistence with the findings in previous studies.[9,12]

We next study the weak in-plane magnetic behavior in Fe_4GeTe_2 near T_c (∼264.4 K; see Figure 3b). It is well-known that thermal fluctuations at temperatures slightly below T_c can lead to random switching of the magnetizations.[39−41] However, for the in-plane case, it has not been reported in the previous literature as being limited by the sensitivity of the magnetometer. Since the free energy of ferromagnets can be described by a GL model for continuous phase transformation in an infinite system,[49] a general picture of the in-plane magnetization escape process is presented in Figure 4a. This process is in contrast to the out-of-plane escape process reported in our recent work.[35] For a GL model with isotropic interactions, the magnetization may occur in any direction along the Mexican hat potential, in which the in-plane magnetization driven by thermal fluctuations should randomly rotate within the minimal potential (see Figure 4b). Instead, in the presence of in-plane anisotropy, the in-plane magnetization should randomly choose one of the local minima, leading to well-defined in-plane polarization along two particular directions.

With the above idea, we use the three-point sampling method[50] instead of the full ODMR spectrum to obtain the thermally activated escape process, in which the external magnetic bias field is tuned along the out-of-plane direction with B_{bias}^{z} = 1.3 mT (see Section II in the Supporting Information). In this case, the in-plane field almost vanishes with $B_{bias}^{xy} = 0$. Figure 4c shows the z axis component B_{bias}^{z} of the

https://doi.org/10.1021/acs.nanolett.4c00795
Nano Lett. 2024, 24, 5754−5760

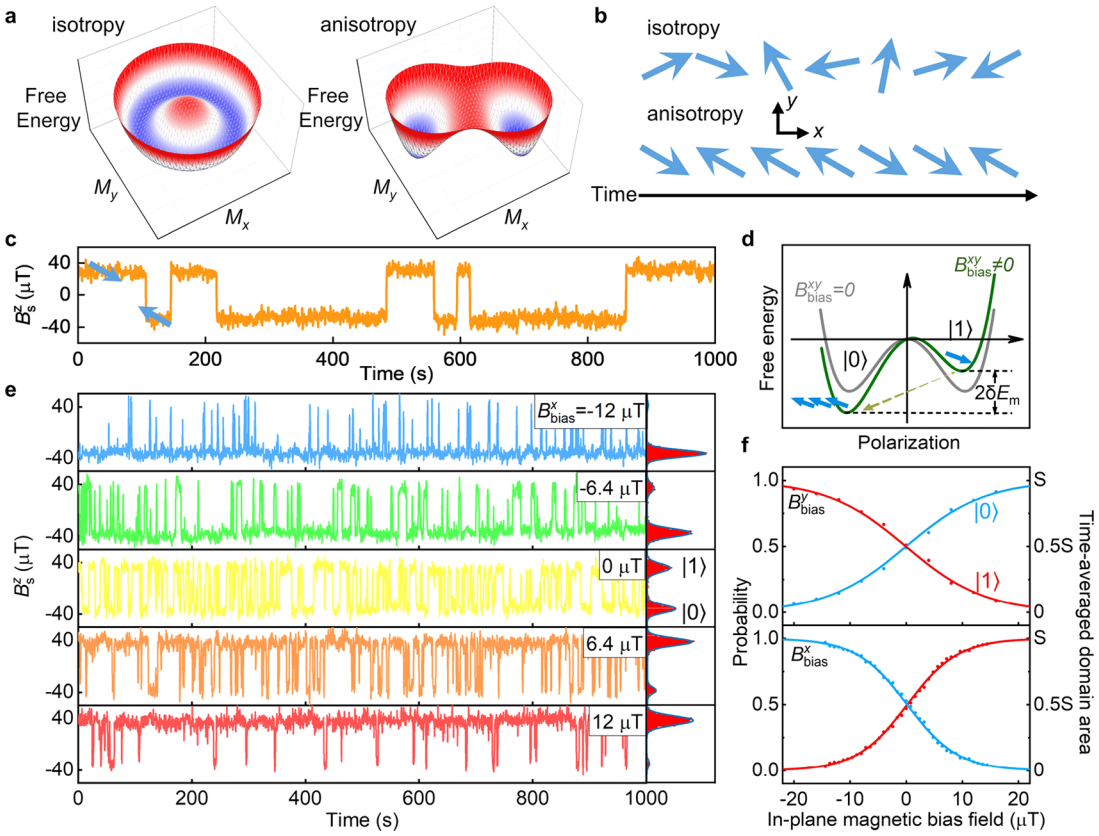

Figure 4. Thermal-activated escape, in-plane magnetization, and anisotropy in Fe_4GeTe_2. (a) Free energy landscape without (left) and with (right) in-plane anisotropy. (b) Schematic of the varied magnetization direction with time under in-plane isotropic and anisotropic conditions during thermal escape process. (c) Time traces of the stray magnetic field B_s^z. The in-plane magnetization switches between two states. (d) Schematic of the GL double-well model under different external magnetic fields. The green and gray lines indicate the presence and absence of an external magnetic field, respectively. (e) Time traces of B_s^z at different B_{bias}^x. The right panels are histograms of the B_s^z, and the blue curves are fitted with double Gauss peaks. (f) Probability and time-averaged domain area of state $|1\rangle$ (red line) and state $|0\rangle$ (blue line) at different B_{bias}^x and B_{bias}^y. The solid lines are the fittings using eq 1, and the dots are experimental data.

sample as a function of time (0.5 s per data point) at 254.9 K, revealing that there are only two discrete jumping states, representing the two spin directions (termed $|0\rangle$ and $|1\rangle$). By the measured stray magnetic field from the flake, we estimate that the two states are antiparallel to the azimuth angles $\varphi_{|0\rangle} \approx 150°$ and $\varphi_{|1\rangle} \approx 330°$ (see Section IV in the Supporting Information). This result provides unique evidence that Fe_4GeTe_2 also exhibits some kind of in-plane anisotropy. Furthermore, we find that the probability of the spin occurring in these two states is the same, suggesting that the two minima have the same depth, giving rise to $\mathbb{Z}_2$ symmetry.

To further check the in-plane anisotropy in Fe_4GeTe_2, we apply a weak in-plane magnetic field to tune the relative depth of the two potential minima $2\delta E_m$.[39] A magnetic field parallel or antiparallel to the spin direction will cause a change in the relative depth of the two potentials, which affects the occupation probability and dwell time in these two states (Figure 4d). The probabilities in states $|0\rangle$ and $|1\rangle$, P_0 and P_1, satisfy the Boltzmann distribution law as

$$P_0/P_1 = e^{2\delta E_m/k_B T} \tag{1}$$

where k_B is the Boltzmann constant. As shown in Figure 4c, under a zero in-plane magnetic field the probabilities of the two states are the same with $2\delta E_m \approx 0$. Because the out-of-plane magnetic field will not affect the in-plane potential depth, we have

$$2\delta E_m = 2mB_{bias}^{x,y}\cos\langle \boldsymbol{e}_{x,y}, \boldsymbol{e}_{|0\rangle}\rangle \tag{2}$$

where $B_{bias}^{x,y}$ is the in-plane projection of $\mathbf{B}_{bias}$ along the x axis or y axis and $\boldsymbol{e}_{x,y}$ and $\boldsymbol{e}_{|0\rangle}$ are the unit vectors of x axis, y axis, and state in the $|0\rangle$ direction. As shown in Figure 4e, we adjust the in-plane projection of $\mathbf{B}_{bias}$ to be along the y axis and change B_{bias}^x. The histogram on the right side of Figure 4e shows a clear change in the occupation probability influenced by B_{bias}^x. According to eqs 1 and 2, the fitting results are shown in Figure 4f, where we find $2m\cos\langle \boldsymbol{e}_x, \boldsymbol{e}_{|0\rangle}\rangle = -4.88$ meV μT^{-1}. Similarly, we adjust the in-plane projection of $\mathbf{B}_{bias}$ to be along the y axis and change B_{bias}^y. We find that the change in the direction of $\mathbf{B}_{bias}$ hardly changed the directions of the magnetization in states $|0\rangle$ and $|1\rangle$, suggesting that differently oriented in-plane bias fields do not change the in-plane anisotropic direction (see Figure S6b,c in the Supporting Information). As shown in Figure 4f, we obtain $2m\cos\langle \boldsymbol{e}_y, \boldsymbol{e}_{|0\rangle}\rangle = 3.10$ meV μT^{-1}. Therefore, we get the results of $\langle \boldsymbol{e}_x, \boldsymbol{e}_{|0\rangle}\rangle = 147.5°$, which is very close to our estimation of the azimuth angle at 150°, and $m = 2.89$ meV μT^{-1}.

The magnetization intensity m can be estimated in another way using the magnetic domain area. For a domain size $S \approx 4$ μm^2 and a magnetization area density of ~ 12 μ_B nm^{-2} (see Figure S6 in the Supporting Information), we have $m \sim 4.8 \times 10^7$ μ_B. Considering that 1 $\mu_B = 5.8 \times 10^{-5}$ eV T^{-1}, $m \approx 2.8$ meV μT^{-1} is obtained. The m and $\langle \boldsymbol{e}_x, \boldsymbol{e}_{|0\rangle}\rangle$ values obtained using different approaches are very close to each other. As

https://doi.org/10.1021/acs.nanolett.4c00795
Nano Lett. 2024, 24, 5754−5760

given in Section VII in the Supporting Information, we also studied the temperature-dependent thermally activated escape process. These results justify the validity of the in-plane anisotropic GL model and the consistency of our experimental method.

In our experiment, a C_3 symmetry is expected for a perfect Fe_4GeTe_2 from the crystal symmetry. For 2D magnets, the typical anisotropic energy is $K_{eff} \approx 0.001-0.1$ meV per magnetic atom,[9,12] which is much higher than our results ($2\delta E_m \approx 10^{-7}$ meV per Fe atom at $B^x_{bias} = 25$ μT). Nevertheless, the in-plane magnetic anisotropy may come from magnetic anisotropy typically arising from the magnetocrystalline, shape, stress (magnetoelastic), and exchange anisotropy. The C_3 symmetry is expected for a perfect Fe_4GeTe_2, making it unlikely to possess 2-fold magnetocrystalline anisotropy. The exchange anisotropy typically occurs during interactions between antiferromagnetic and ferromagnetic materials, which are not present in our sample. Furthermore, considering the absence of a distinct aspect ratio in our sample and the consistent in-plane anisotropy orientation observed both at the sample edge and interior (see Figures S5 and S6), the possibility of shape anisotropy effect can be basically excluded. Therefore, we conjecture that the stress plays a main role in the observed in-plane magnetic anisotropy. The stress anisotropy may come from the lattice mismatch effect with the hBN substrate, which can distort the sample along a particular direction.

Microscopically, the observed $2\delta E_m$ under weak magnetic field tuning allows the exploration of subtle formation of magnetic domains near the phase transition. In Figure 4f, we define the effective area of magnetization with the two states as P_1S and P_0S. The variation of the domain area as a function of external magnetic field is then reflected using $(P_1 - P_0)S/B^{xy}_{bias}$, which is estimated to be about 0.40 μm^2 μT^{-1} when the in-plane component of $\mathbf{B}_{bias}$ is parallel to the x axis and -0.26 μm^2 μT^{-1} when the in-plane component of $\mathbf{B}_{bias}$ is parallel to the y axis (see Section VIII in the Supporting Information). For our study near T_c, this result directly visualizes the ability of the magnetic field to induce domain nucleation at the phase transition for ultrathin Fe_4GeTe_2.

To conclude, we quantitatively investigate the magnetization of the 2D ferromagnet Fe_4GeTe_2 using a nonperturbative NV magnetometer.[33,35] By imaging the stray field of the bilayer Fe_4GeTe_2 at different temperatures, we can determine the surface magnetization and its associated anisotropy. We determine the SRT at approximately 80 K and the thermally activated escape process of the in-plane magnetization slightly below T_c at ~264.4 K. Our results demonstrate that the anisotropy of this system in all the 3D directions is important and observable. Our approach can serve as a unique tool for studying the magnetization anisotropy in a vast number of 2D magnets, which should facilitate the refinement of the theoretical modeling of these materials in the future.[51−53] In particular, in the presence of anisotropy in all directions, the effective Stoner−Wohlfarth model[48] needs to be refined accordingly.

■ ASSOCIATED CONTENT

Data Availability Statement

The data that support the findings of this study are available from the corresponding author upon reasonable request.

Supporting Information

The Supporting Information is available free of charge at https://pubs.acs.org/doi/10.1021/acs.nanolett.4c00795.

Additional results and details for sample preparation, applied bias magnetic field, characterization of Fe_4GeTe_2 crystal, observed magnetization fluctuation, temperature-dependent Ginzburg−Landau model, analysis of field-dependent domain area, and the calculation of effective magnetic anisotropy energy (PDF)

■ AUTHOR INFORMATION

Corresponding Authors

Fazhan Shi − *International Center for Quantum Design of Functional Materials (ICQD), Hefei National Research Center for Physical Science at the Microscale, University of Science and Technology of China, Hefei, Anhui 230026, People's Republic of China; CAS Key Laboratory of Microscale Magnetic Resonance, University of Science and Technology of China, Hefei, Anhui 230026, People's Republic of China; Hefei National Laboratory, University of Science and Technology of China, Hefei 230088, People's Republic of China*; Email: fzshi@ustc.edu.cn

Ming Gong − *CAS Key Laboratory of Quantum Information and CAS Center For Excellence in Quantum Information and Quantum Physics, University of Science and Technology of China, Hefei, Anhui 230026, People's Republic of China; Hefei National Laboratory, University of Science and Technology of China, Hefei 230088, People's Republic of China*; Email: gongm@ustc.edu.cn

Hualing Zeng − *International Center for Quantum Design of Functional Materials (ICQD), Hefei National Research Center for Physical Science at the Microscale, University of Science and Technology of China, Hefei, Anhui 230026, People's Republic of China; CAS Key Laboratory of Strongly Coupled Quantum Matter Physics, Department of Physics, University of Science and Technology of China, Hefei, Anhui 230026, People's Republic of China; Hefei National Laboratory, University of Science and Technology of China, Hefei 230088, People's Republic of China*; orcid.org/0000-0001-5869-9553; Email: hlzeng@ustc.edu.cn

Authors

Chen Wang − *International Center for Quantum Design of Functional Materials (ICQD), Hefei National Research Center for Physical Science at the Microscale, University of Science and Technology of China, Hefei, Anhui 230026, People's Republic of China; CAS Key Laboratory of Strongly Coupled Quantum Matter Physics, Department of Physics, University of Science and Technology of China, Hefei, Anhui 230026, People's Republic of China; Hefei National Laboratory, University of Science and Technology of China, Hefei 230088, People's Republic of China*

Siyuan Wan − *School of Physics and Materials Science, Nanchang University, Nanchang 330031, People's Republic of China*

Ya Wang − *International Center for Quantum Design of Functional Materials (ICQD), Hefei National Research Center for Physical Science at the Microscale, University of Science and Technology of China, Hefei, Anhui 230026, People's Republic of China; CAS Key Laboratory of Microscale Magnetic Resonance, University of Science and Technology of China, Hefei, Anhui 230026, People's Republic of China; Hefei National Laboratory, University of Science*

https://doi.org/10.1021/acs.nanolett.4c00795
Nano Lett. 2024, 24, 5754−5760

and Technology of China, Hefei 230088, People's Republic of China; orcid.org/0000-0001-6232-7234

Complete contact information is available at: https://pubs.acs.org/10.1021/acs.nanolett.4c00795

Author Contributions

H.Z. conceived the idea and designed the experiments. S.W. prepared the samples. C.W. fabricated the devices and carried out the ODMR measurements. C.W., M.G., and H.Z. analyzed the data and wrote the paper. All the authors commented on the manuscript.

Notes

The authors declare no competing financial interest.

■ ACKNOWLEDGMENTS

This work is supported by the CAS Project for Young Scientists in Basic Research (Grant No. YSBR-049), the Innovation Program for Quantum Science and Technology (Grant Nos. 2021ZD0302800, 2021ZD0301200, and 2021ZD0301500), the National Key Research and Development Program of China (Grant No. 2018YFA0306600), the Fundamental Research Funds for the Central Universities (Grant No. WK3510000013), and the Strategic Priority Research Program of the Chinese Academy of Sciences (Grant No. XDB0500000). This work was partially carried out at the USTC Center for Micro and Nanoscale Research and Fabrication.

■ REFERENCES

(1) Gong, C.; Li, L.; Li, Z.; Ji, H.; Stern, A.; Xia, Y.; Cao, T.; Bao, W.; Wang, C.; Wang, Y.; Qiu, Z. Q.; Cava, R. J.; Louie, S. G.; Xia, J.; Zhang, X. Discovery of intrinsic ferromagnetism in two-dimensional van der Waals crystals. *Nature* **2017**, *546* (7657), 265−269.

(2) Huang, B.; Clark, G.; Navarro-Moratalla, E.; Klein, D. R.; Cheng, R.; Seyler, K. L.; Zhong, D.; Schmidgall, E.; McGuire, M. A.; Cobden, D. H.; Yao, W.; Xiao, D.; Jarillo-Herrero, P.; Xu, X. Layer-dependent ferromagnetism in a van der Waals crystal down to the monolayer limit. *Nature* **2017**, *546* (7657), 270−273.

(3) Bonilla, M.; Kolekar, S.; Ma, Y.; Diaz, H. C.; Kalappattil, V.; Das, R.; Eggers, T.; Gutierrez, H. R.; Phan, M. H.; Batzill, M. Strong room-temperature ferromagnetism in VSe_2 monolayers on van der Waals substrates. *Nat. Nanotechnol.* **2018**, *13* (4), 289−293.

(4) Fei, Z.; Huang, B.; Malinowski, P.; Wang, W.; Song, T.; Sanchez, J.; Yao, W.; Xiao, D.; Zhu, X.; May, A. F.; Wu, W.; Cobden, D. H.; Chu, J. H.; Xu, X. Two-dimensional itinerant ferromagnetism in atomically thin Fe_3GeTe_2. *Nat. Mater.* **2018**, *17* (9), 778−782.

(5) Wang, Z.; Sapkota, D.; Taniguchi, T.; Watanabe, K.; Mandrus, D.; Morpurgo, A. F. Tunneling spin valves based on Fe_3GeTe_2/hBN/Fe_3GeTe_2 van der Waals heterostructures. *Nano Lett.* **2018**, *18* (7), 4303−4308.

(6) Ostwal, V.; Shen, T.; Appenzeller, J. Efficient spin-orbit torque switching of the semiconducting van der Waals ferromagnet $Cr_2Ge_2Te_6$. *Adv. Mater.* **2020**, *32* (7), No. e1906021.

(7) Chen, G.; Qi, S.; Liu, J.; Chen, D.; Wang, J.; Yan, S.; Zhang, Y.; Cao, S.; Lu, M.; Tian, S.; Chen, K.; Yu, P.; Liu, Z.; Xie, X. C.; Xiao, J.; Shindou, R.; Chen, J. H. Electrically switchable van der Waals magnon valves. *Nat. Commun.* **2021**, *12* (1), 6279.

(8) May, A. F.; Ovchinnikov, D.; Zheng, Q.; Hermann, R.; Calder, S.; Huang, B.; Fei, Z.; Liu, Y.; Xu, X.; McGuire, M. A. Ferromagnetism near room temperature in the cleavable van der Waals crystal Fe_5GeTe_2. *ACS Nano* **2019**, *13* (4), 4436−4442.

(9) Seo, J.; Kim, D. Y.; An, E. S.; Kim, K.; Kim, G. Y.; Hwang, S. Y.; Kim, D. W.; Jang, B. G.; Kim, H.; Eom, G.; Seo, S. Y.; Stania, R.; Muntwiler, M.; Lee, J.; Watanabe, K.; Taniguchi, T.; Jo, Y. J.; Lee, J.; Min, B. I.; Jo, M. H.; Yeom, H. W.; Choi, S. Y.; Shim, J. H.; Kim, J. S. Nearly room temperature ferromagnetism in a magnetic metal-rich van der Waals metal. *Sci. Adv.* **2020**, *6* (3), No. eaay8912.

(10) Kim, D.; Lee, C.; Jang, B. G.; Kim, K.; Shim, J. H. Drastic change of magnetic anisotropy in Fe_3GeTe_2 and Fe_4GeTe_2 monolayers under electric field studied by density functional theory. *Sci. Rep* **2021**, *11* (1), 17567.

(11) Yang, X.; Zhou, X.; Feng, W.; Yao, Y. Strong magneto-optical effect and anomalous transport in the two-dimensional van der Waals magnets Fe_nGeTe_2 (n = 3, 4, 5). *Phys. Rev. B* **2021**, *104* (10), 104427.

(12) Wang, H.; Lu, H.; Guo, Z.; Li, A.; Wu, P.; Li, J.; Xie, W.; Sun, Z.; Li, P.; Damas, H.; Friedel, A. M.; Migot, S.; Ghanbaja, J.; Moreau, L.; Fagot-Revurat, Y.; Petit-Watelot, S.; Hauet, T.; Robertson, J.; Mangin, S.; Zhao, W.; Nie, T. Interfacial engineering of ferromagnetism in wafer-scale van der Waals Fe_4GeTe_2 far above room temperature. *Nat. Commun.* **2023**, *14* (1), 2483.

(13) Rana, D.; Bhakar, M.; G, B.; Bera, S.; Saini, N.; Pradhan, S. K.; Mondal, M.; Kabir, M.; Sheet, G. High transport spin polarization in the van der Waals ferromagnet Fe_4GeTe_2. *Phys. Rev. B* **2023**, *107* (22), 224422.

(14) Chen, H.; Asif, S.; Whalen, M.; Támara-Isaza, J.; Luetke, B.; Wang, Y.; Wang, X.; Ayako, M.; Lamsal, S.; May, A. F.; et al. Revealing room temperature ferromagnetism in exfoliated Fe_5GeTe_2 flakes with quantum magnetic imaging. *2D Mater.* **2022**, *9* (2), 025017.

(15) Robertson, I. O.; Tan, C.; Scholten, S. C.; Healey, A. J.; Abrahams, G. J.; Zheng, G.; Manchon, A.; Wang, L.; Tetienne, J.-P. Imaging current control of magnetization in Fe_3GeTe_2 with a widefield nitrogen-vacancy microscope. *2D Mater.* **2023**, *10* (1), 015023.

(16) Chen, H.; Asif, S.; Dolui, K.; Wang, Y.; Támara-Isaza, J.; Goli, V. D. P.; Whalen, M.; Wang, X.; Chen, Z.; Zhang, H.; et al. Above-room-temperature ferromagnetism in thin van der Waals flakes of cobalt-substituted Fe_5GeTe_2. *ACS Appl. Mater. Interfaces* **2023**, *15* (2), 3287−3296.

(17) Huang, M.; Zhou, J.; Chen, D.; Lu, H.; McLaughlin, N. J.; Li, S.; Alghamdi, M.; Djugba, D.; Shi, J.; Wang, H.; et al. Wide field imaging of van der Waals ferromagnet Fe_3GeTe_2 by spin defects in hexagonal boron nitride. *Nat. Commun.* **2022**, *13* (1), 5369.

(18) Bera, S.; Pradhan, S. K.; Khan, M. S.; Pal, R.; Pal, B.; Kalimuddin, S.; Bera, A.; Das, B.; Pal, A. N.; Mondal, M. Unravelling the nature of spin reorientation transition in quasi-2D vdW magnetic material, Fe_4GeTe_2. *J. Magn. Magn. Mater.* **2023**, *565*, 170257.

(19) Deng, Y.; Yu, Y.; Song, Y.; Zhang, J.; Wang, N. Z.; Sun, Z.; Yi, Y.; Wu, Y. Z.; Wu, S.; Zhu, J.; Wang, J.; Chen, X. H.; Zhang, Y. Gate-tunable room-temperature ferromagnetism in two-dimensional Fe_3GeTe_2. *Nature* **2018**, *563* (7729), 94−99.

(20) Qin, Y.; Shen, Y.; Liu, C.; Wo, H.; Gao, Y.; Feng, Y.; Zhang, X.; Ding, G.; Gu, Y.; Wang, Q.; Shen, S.; Walker, H. C.; Bewley, R.; Xu, J.; Boehm, M.; Steffens, P.; Ohira-Kawamura, S.; Murai, N.; Schneidewind, A.; Tong, X.; Chen, G.; Zhao, J. Field-tuned quantum effects in a triangular-lattice Ising magnet. *Sci. Bull.* **2022**, *67* (1), 38−44.

(21) Gibertini, M.; Koperski, M.; Morpurgo, A. F.; Novoselov, K. S. Magnetic 2D materials and heterostructures. *Nat. Nanotechnol.* **2019**, *14* (5), 408−419.

(22) Xing, S.; Zhou, J.; Zhang, X.; Elliott, S.; Sun, Z. Theory, properties and engineering of 2D magnetic materials. *Prog. Mater. Sci.* **2023**, *132*, 101036.

(23) Gruber, A.; Drabenstedt, A.; Tietz, C.; Fleury, L.; Wrachtrup, J.; vonBorczyskowski, C. Scanning confocal optical microscopy and magnetic resonance on single defect centers. *Science* **1997**, *276* (5321), 2012−2014.

(24) Rondin, L.; Tetienne, J. P.; Hingant, T.; Roch, J. F.; Maletinsky, P.; Jacques, V. Magnetometry with nitrogen-vacancy defects in diamond. *Rep. Prog. Phys.* **2014**, *77* (5), 056503.

(25) Schirhagl, R.; Chang, K.; Loretz, M.; Degen, C. L. Nitrogen-vacancy centers in diamond: nanoscale sensors for physics and biology. *Annu. Rev. Phys. Chem.* **2014**, *65*, 83−105.

(26) Casola, F.; van der Sar, T.; Yacoby, A. Probing condensed matter physics with magnetometry based on nitrogen-vacancy centres in diamond. *Nat. Rev. Mater.* **2018**, *3* (1), 1−13.
(27) Mitchell, M. W.; Alvarez, S. P. Colloquium: Quantum limits to the energy resolution of magnetic field sensors. *Rev. Mod. Phys.* **2020**, *92* (2), 021001.
(28) Xu, Y.; Zhang, W.; Tian, C. Recent advances on applications of NV^- magnetometry in condensed matter physics. *Photonics Res.* **2023**, *11* (3), 393−412.
(29) Toyli, D. M.; Christle, D. J.; Alkauskas, A.; Buckley, B. B.; Van de Walle, C. G.; Awschalom, D. D. Measurement and control of single nitrogen-vacancy center spins above 600 K. *Phys. Rev. X* **2012**, *2* (3), 031001.
(30) Doherty, M. W.; Acosta, V. M.; Jarmola, A.; Barson, M. S. J.; Manson, N. B.; Budker, D.; Hollenberg, L. C. L. Temperature shifts of the resonances of the NV^- center in diamond. *Phys. Rev. B* **2014**, *90* (4), 041201.
(31) Balasubramanian, G.; Neumann, P.; Twitchen, D.; Markham, M.; Kolesov, R.; Mizuochi, N.; Isoya, J.; Achard, J.; Beck, J.; Tissler, J.; Jacques, V.; Hemmer, P. R.; Jelezko, F.; Wrachtrup, J. Ultralong spin coherence time in isotopically engineered diamond. *Nat. Mater.* **2009**, *8* (5), 383−387.
(32) Wolf, T.; Neumann, P.; Nakamura, K.; Sumiya, H.; Ohshima, T.; Isoya, J.; Wrachtrup, J. Subpicotesla diamond magnetometry. *Phys. Rev. X* **2015**, *5* (4), 041001.
(33) Thiel, L.; Wang, Z.; Tschudin, M. A.; Rohner, D.; Gutierrez-Lezama, I.; Ubrig, N.; Gibertini, M.; Giannini, E.; Morpurgo, A. F.; Maletinsky, P. Probing magnetism in 2D materials at the nanoscale with single-spin microscopy. *Science* **2019**, *364* (6444), 973−976.
(34) Sun, Q. C.; Song, T.; Anderson, E.; Brunner, A.; Forster, J.; Shalomayeva, T.; Taniguchi, T.; Watanabe, K.; Grafe, J.; Stohr, R.; Xu, X.; Wrachtrup, J. Magnetic domains and domain wall pinning in atomically thin $CrBr_3$ revealed by nanoscale imaging. *Nat. Commun.* **2021**, *12* (1), 1989.
(35) Broadway, D. A.; Scholten, S. C.; Tan, C.; Dontschuk, N.; Lillie, S. E.; Johnson, B. C.; Zheng, G.; Wang, Z.; Oganov, A. R.; Tian, S.; Li, C.; Lei, H.; Wang, L.; Hollenberg, L. C. L.; Tetienne, J. P. Imaging domain reversal in an ultrathin van der Waals ferromagnet. *Adv. Mater.* **2020**, *32* (39), 2003314.
(36) Song, T.; Sun, Q. C.; Anderson, E.; Wang, C.; Qian, J.; Taniguchi, T.; Watanabe, K.; McGuire, M. A.; Stohr, R.; Xiao, D.; Cao, T.; Wrachtrup, J.; Xu, X. Direct visualization of magnetic domains and moire magnetism in twisted 2D magnets. *Science* **2021**, *374* (6571), 1140−1144.
(37) Dubois, A. E. E.; Broadway, D. A.; Stark, A.; Tschudin, M. A.; Healey, A. J.; Huber, S. D.; Tetienne, J. P.; Greplova, E.; Maletinsky, P. Untrained physically informed neural network for image reconstruction of magnetic field sources. *Phys. Rev. Appl.* **2022**, *18* (6), 064076.
(38) Broadway, D. A.; Lillie, S. E.; Scholten, S. C.; Rohner, D.; Dontschuk, N.; Maletinsky, P.; Tetienne, J. P.; Hollenberg, L. C. L. Improved current density and magnetization reconstruction through vector magnetic field measurements. *Phys. Rev. Appl.* **2020**, *14* (2), 024076.
(39) Wang, C.; Kong, X.; Mao, X.; Chen, C.; Yu, P.; Wang, Y.; Shi, F.; Du, J.; Gong, M.; Zeng, H. Thermal-activated escape of the bistable magnetic states in 2D Fe_3GeTe_2 near the critical point. *Commun. Phys.* **2023**, *6* (1), 351.
(40) Rondin, L.; Gieseler, J.; Ricci, F.; Quidant, R.; Dellago, C.; Novotny, L. Direct measurement of Kramers turnover with a levitated nanoparticle. *Nat. Nanotechnol.* **2017**, *12* (12), 1130−1133.
(41) McCann, L. I.; Dykman, M.; Golding, B. Thermally activated transitions in a bistable three-dimensional optical trap. *Nature* **1999**, *402* (6763), 785−787.
(42) Meyer, E.; Hug, H. J.; Bennewitz, R. *Scanning probe microscopy*; Springer: 2003; Vol. *4*.
(43) Tetienne, J. P.; Broadway, D. A.; Lillie, S. E.; Dontschuk, N.; Teraji, T.; Hall, L. T.; Stacey, A.; Simpson, D. A.; Hollenberg, L. C. L. Proximity-induced artefacts in magnetic imaging with nitrogen-vacancy ensembles in diamond. *Sensors* **2018**, *18* (4), 1290.
(44) Balasubramanian, G.; Chan, I. Y.; Kolesov, R.; Al-Hmoud, M.; Tisler, J.; Shin, C.; Kim, C.; Wojcik, A.; Hemmer, P. R.; Krueger, A.; Hanke, T.; Leitenstorfer, A.; Bratschitsch, R.; Jelezko, F.; Wrachtrup, J. Nanoscale imaging magnetometry with diamond spins under ambient conditions. *Nature* **2008**, *455* (7213), 648−651.
(45) Rondin, L.; Tetienne, J. P.; Spinicelli, P.; Dal Savio, C.; Karrai, K.; Dantelle, G.; Thiaville, A.; Rohart, S.; Roch, J. F.; Jacques, V. Nanoscale magnetic field mapping with a single spin scanning probe magnetometer. *Appl. Phys. Lett.* **2012**, *100* (15), 153118.
(46) Lesik, M.; Plisson, T.; Toraille, L.; Renaud, J.; Occelli, F.; Schmidt, M.; Salord, O.; Delobbe, A.; Debuisschert, T.; Rondin, L.; Loubeyre, P.; Roch, J. F. Magnetic measurements on micrometer-sized samples under high pressure using designed NV centers. *Science* **2019**, *366* (6471), 1359−1362.
(47) Tetienne, J. P.; Dontschuk, N.; Broadway, D. A.; Stacey, A.; Simpson, D. A.; Hollenberg, L. C. L. Quantum imaging of current flow in graphene. *Sci. Adv.* **2017**, *3* (4), No. e1602429.
(48) Tang, M.; Huang, J.; Qin, F.; Zhai, K.; Ideue, T.; Li, Z.; Meng, F.; Nie, A.; Wu, L.; Bi, X.; Zhang, C.; Zhou, L.; Chen, P.; Qiu, C.; Tang, P.; Zhang, H.; Wan, X.; Wang, L.; Liu, Z.; Tian, Y.; Iwasa, Y.; Yuan, H. Continuous manipulation of magnetic anisotropy in a van der Waals ferromagnet via electrical gating. *Nat. Electron.* **2022**, *6* (1), 28−36.
(49) Altland, A.; Simons, B. D. *Condensed matter field theory*; Cambridge University Press: 2010.
(50) Tzeng, Y. K.; Tsai, P. C.; Liu, H. Y.; Chen, O. Y.; Hsu, H.; Yee, F. G.; Chang, M. S.; Chang, H. C. Time-resolved luminescence nanothermometry with nitrogen-vacancy centers in nanodiamonds. *Nano Lett.* **2015**, *15* (6), 3945−3952.
(51) Burch, K. S.; Mandrus, D.; Park, J. G. Magnetism in two-dimensional van der Waals materials. *Nature* **2018**, *563* (7729), 47−52.
(52) Kurebayashi, H.; Garcia, J. H.; Khan, S.; Sinova, J.; Roche, S. Magnetism, symmetry and spin transport in van der Waals layered systems. *Nat. Rev. Phys.* **2022**, *4* (3), 150−166.
(53) Gong, C.; Zhang, X. Two-dimensional magnetic crystals and emergent heterostructure devices. *Science* **2019**, *363* (6428), No. eaav4450.

https://doi.org/10.1021/acs.nanolett.4c00795
Nano Lett. 2024, 24, 5754−5760